ACS ES&T Water

pubs.acs.org/estwater

Article

Seasonal Lead Release into Drinking Water and the Effect of Aluminum

Benjamin F. Trueman,* Aaron Bleasdale-Pollowy, Javier A. Locsin, Jessica L. Bennett, Wendy H. Krkošek, and Graham A. Gagnon

Cite This: *ACS EST Water* 2022, 2, 710−720

Read Online

ACCESS | Metrics & More | Article Recommendations | Supporting Information

ABSTRACT: Monitoring lead in drinking water is important for public health, but seasonality in lead concentrations can bias monitoring programs if it is not understood and accounted for. Here, we describe an apparent seasonal pattern in lead release into orthophosphate-treated drinking water, identified through point-of-use sampling at sites in Halifax, Canada, with various sources of lead. Using a generalized additive model, we extracted the seasonally varying components of time series representing a suite of water quality parameters and we identified aluminum as a correlate of lead. To investigate aluminum's role in lead release, we modeled the effect of variscite ($AlPO_4{\cdot}2H_2O$) precipitation on lead solubility, and we evaluated the effects of aluminum, temperature, and orthophosphate concentration on lead release from new lead coupons. At environmentally relevant aluminum and orthophosphate concentrations, variscite precipitation increased predicted lead solubility by decreasing available orthophosphate. Increasing the aluminum concentration from 20 to 500 $\mu g\ L^{-1}$ increased lead release from coupons by 41% and modified the effect of orthophosphate, rendering it less effective. We attributed this to a decrease in the concentration of soluble (<0.45 μm) phosphorus with increasing aluminum and an accompanying increase in particulate lead and phosphorus (>0.45 μm).

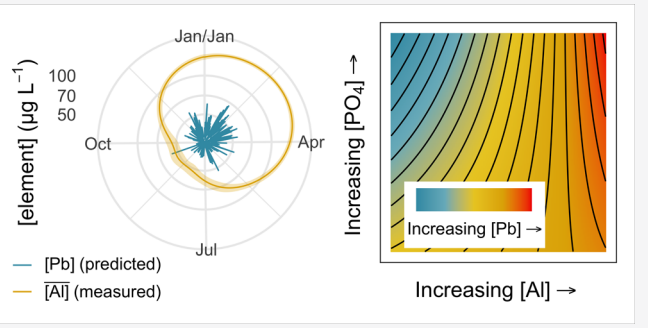

KEYWORDS: *Variscite, PHREEQC, generalized additive model, orthophosphate, mgcv, coagulation*

INTRODUCTION

Lead is a contaminant of concern in drinking water due to its well-documented health effects.[1,2] Many jurisdictions require that it be monitored, but seasonal variation in lead release can bias monitoring programs if it is not understood and accounted for. Temperature-driven lead seasonality has been described in previous work,[3] and sampling guidance is often designed to control for temperature effects.[4]

But water quality parameters other than temperature can contribute to seasonal lead concentrations, and aluminum is an important example. Aluminum concentrations can vary seasonally when water is treated to remove particles and dissolved organic matter by coagulation. This is because the solubility of aluminum hydroxide [$Al(OH)_3$] that precipitates during coagulation with aluminum salts is highly temperature-dependent. Below the minimum solubility at pH 6−7,[5] solubility decreases with the increasing temperature, and above pH 6−7, solubility increases with temperature.[6] Treatment facilities that coagulate below the pH of minimum solubility, then, tend to yield high residual aluminum in winter. Facilities that coagulate at alkaline pH may yield high residual aluminum in summer.[7]

This in turn may influence lead release, but the complex environment of a drinking water distribution system and the possibility of multiple competing mechanisms make it difficult to predict aluminum's net effect. Aluminum might precipitate at the scale−water interface as a hydroxide or silicate mineral that slows lead diffusion to the bulk water,[8−11] but this is controversial.[12,13] It might also precipitate as a phosphate mineral, diminishing the activity of orthophosphate and preventing the formation of hydroxypyromorphite [$Pb_5(PO_4)_3OH$] and other low-solubility phases that control lead release.[5,11,14−18] Aluminum precipitation that results in suspended particles or colloids may generate a mobile sink for lead, facilitating lead transport from source to tap.[19−21]

Here, we consider aluminum and other seasonally varying water quality parameters as drivers of seasonal lead release. We use a hybrid approach that combines statistical analysis of observational data, a factorial experiment, and a mechanistic model. We identify possible origins of periodic lead release in the distribution system of Halifax, a mid-sized North American

Received: September 3, 2021
Revised: April 6, 2022
Accepted: April 7, 2022
Published: April 20, 2022

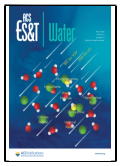

https://doi.org/10.1021/acsestwater.1c00320
ACS EST Water 2022, 2, 710−720

Table 1. Data Sources, Sample Sizes, and Figures in Which Specific Data Sets Appear

data source	analytes	appears in Figures	source
volunteer-collected 1 L flushed samples	total Al (n = 849), 0.45 μm filtered Al (n = 362)	2, 4b, 7c	utility data
plant/distribution system monitoring data	Al (n = 1217), PO_4 (n = 2708), temperature (n = 1595), alkalinity (n = 414), pH (n = 414), orthophosphate product dose (n = 6035)	2, 7c	utility data
volunteer-collected 1 L profile samples	Pb, Cu (n = 360 per parameter)	S11	utility data
volunteer-collected 1 L profile samples	Al, Fe, Pb, via SEC-ICP-MS (n = 16)	4a	doi.org/10.5281/zenodo.5139734
residential 1 L first-draw and flushed samples	Pb (n = 193), Cu (n = 193), pH (n = 125), temperature (n = 86), turbidity (n = 192)	3	McIlwain[25] and doi.org/10.5281/zenodo.5139734
nonresidential 0.25 L first-draw and flushed samples	Pb (n = 303), Cu (n = 303), pH (n = 232), temperature (n = 148), turbidity (n = 303)	3	McIlwain[25] and doi.org/10.5281/zenodo.5139734
coupon study	total Pb, Al, P (n = 128 per parameter); 0.45 μm filtered Pb, Al, P (n = 32 per parameter)	5	doi.org/10.5281/zenodo.5139734

city, and we isolate a subset of these—aluminum, orthophosphate, and temperature—for investigation using a lead coupon study and a geochemical solubility model. We find that interactions between orthophosphate and aluminum have an important effect on lead release and that variation in aluminum concentrations may play a key role in observed lead concentrations. In our view, mechanisms involving soluble, colloidal, and particulate lead are all relevant to this phenomenon.

MATERIALS AND METHODS

Field Sample Collection. *Distribution System Monitoring.* Distribution system samples were collected by utility staff as part of a routine, long-term monitoring program designed to understand the state of the system and respond to water quality issues. Temperature and pH were measured in the field (Hach PH281 probe), and samples were sent to a third-party accredited laboratory for determination of alkalinity,[22] total aluminum,[23] and orthophosphate.[24]

Point-of-Use Corrosion Control Monitoring. The point-of-use corrosion control monitoring data set represents two distinct monitoring programs, described in McIlwain[25] and Trueman et al.[26] The first comprised samples collected at residential (1 L volume) and nonresidential (0.25 L volume) sites in the distribution system after a minimum 8 h stagnation period (Table 1).[25] Samples were collected over 3 years (2010−2012), representing two October and two February collection periods. This program was designed to evaluate the utility's corrosion control program and to identify outlets with high lead levels. The 34 residential sites included three and six with full and partial lead service lines, respectively. A further 18 had copper service lines, and the remaining 7 had unknown configurations. Outlets used for drinking or cooking were sampled in 48 nonresidential buildings.[25]

The second program was designed to evaluate the effect of lead service line replacement on lead levels in tap water.[26] Volunteer residents collected 1 L samples as 4 × 1 L minimum 6 h stagnant profiles with the addition of a 5 min flushed sample after each profile (Table 1). We filtered a subset of these using 0.45 μm membrane filters in a syringe-mounted apparatus. To quantify aluminum in the distribution system, we used 5 min flushed samples only, thereby minimizing the impact of site-specific factors (e.g., premise plumbing). To estimate particulate lead and copper, we used samples collected before replacement because extreme particulate lead release is typical immediately after replacement.

All samples were collected in high-density polyethylene (HDPE) bottles, cleaned by immersion in ∼2 M HNO_3 for at least 24 h and rinsed thoroughly with ultrapure water. Aluminum, lead, copper, and phosphorus were determined by ICP−MS (Thermofisher X series II) according to Standard Method 3125,[27] with reporting limits of 4.0, 0.4, 0.7, and 10 $\mu g\ L^{-1}$, respectively.

Size-Exclusion Chromatography. Relative size distributions of lead, aluminum, and iron were determined for a subset of the profile samples described above (see Point-of-Use Corrosion Control Monitoring), using size-exclusion chromatography with multielement detection (SEC-ICP-MS). The full method is detailed in a previous publication.[20] Briefly, we separated samples on a stationary phase composed of crosslinked agarose and dextran (Superdex 200, 10 × 300 mm, 13 μm particle size, GE Healthcare) with 50 mM tris−HCl (pH 7.3) as the mobile phase. The flow rate was 0.5 mL min^{-1}, and the injection volume was 212 μL. We monitored ^{27}Al, ^{56}Fe, and ^{208}Pb in the column effluent as a function of time by ICP−MS (see Point-of-Use Corrosion Control Monitoring above). The retention volume of thyroglobulin (669 kDa, Stoke's radius 8.5 nm), indicated in chromatograms as a qualitative point of reference, was monitored as ^{127}I. Chromatograms were summarized as the sum of two skewed or exponentially modified Gaussians using the R package *fffprocessr*,[28] as described elsewhere.[29] R code to reproduce the analysis is included in Supporting Information S1, the individual chromatograms are shown in Figure S1, and the data are available at doi.org/10.5281/zenodo.5139734.

Lead Coupon Study. We investigated the effect of three factors—aluminum (0.02 or 0.5 mg Al L^{-1}), orthophosphate (0 or 1 mg $PO_4\ L^{-1}$), and temperature (4 or 21 °C)—on lead release from new lead coupons using a set of batch corrosion cells made with new lead coupons. We evaluated all eight factor combinations (two aluminum concentrations × two orthophosphate concentrations × two water temperatures) as a 2^3 factorial design (Table S1), generating independent estimates of each factor's effect and estimates of the interactions among factors.

Preparation of Test Water. Preparation of test water for the coupon study is summarized in Figure 1. We coagulated untreated source water from the water supply plant with $Al_2(SO_4)_3{\cdot}18H_2O$ (12 mg Al L^{-1}) in a 20 L HDPE plastic container. The coagulant dose was chosen to match the dose applied at the treatment plant supplying the distribution system we studied.

https://doi.org/10.1021/acsestwater.1c00320
ACS EST Water 2022, 2, 710−720

Figure 1. Summary of test water preparation for the coupon study (created at biorender.com).

Immediately after adding the coagulant, water was mixed at approximately 800 rpm for 1 min using a magnetic stirplate (n.b., rpm is nominal and was determined by the stirplate dial setting). Coagulated water was then mixed for 12.5 min each at 600, 500, and 400 rpm. pH was maintained throughout at 6.3 using sodium hydroxide. The flocculated water was allowed to settle overnight, pumped into a separate reservoir, and filtered using a vacuum flask fitted with a 1.5 μm glass-fiber filter membrane.

This procedure reduced total organic carbon (TOC) to 1.8 mg L^{-1} (standard deviation 0.02 mg L^{-1}), from an approximate raw water concentration of 3.8 mg L^{-1} (a summary of untreated water quality is provided in Table S2). TOC samples were collected, headspace-free, in 40 mL clear glass vials and preserved with concentrated phosphoric acid at pH < 2. Vials were washed and then baked at 105 °C for at least 24 h before use, and TOC was quantified using a Shimadzu TOC-V CPH analyzer.[30]

The filtrate was dosed as needed with H_3PO_4, $Al_2(SO_4)_3 \cdot 18H_2O$, and $NaHCO_3$ (5 mg C L^{-1}) to achieve the experimental conditions listed in Table S1. The initial pH for all test waters was adjusted to 7.5 with HNO_3 and NaOH. pH was measured using a combination electrode, and the nominal orthophosphate concentration was verified colorimetrically.[24]

Corrosion Cell Construction. Corrosion cells were constructed by fastening new lead coupons to the lids of 50 mL polypropylene centrifuge tubes with a silicone sealant. Beforehand, coupons (Canada Metal North America, Québec, Canada) were cleaned by immersion for 2 min in 1.8 M HNO_3, followed by thorough rinsing with ultrapure water. This step was repeated afterward with 40 mM HNO_3.

Coupon Conditioning. Corrosion cells were refilled with 50 mL of fresh test water according to the experimental design summarized in Table S1; this volume was chosen to prevent contact with the sealant, while minimizing the headspace. We completed 42 changes of water before beginning to collect data, and each change was followed by a minimum 24 h stagnation period. After conditioning, lead in 0.45 μm filtrate agreed reasonably well with the predicted equilibrium lead solubility, with a mean absolute error of 8 μg L^{-1} at the low level of aluminum, a temperature of 21 °C, and either 0 or 1 mg PO_4 L^{-1}.

Sample Collection. After each 24 h stagnation period, cells were mixed by inverting five times. Aliquots of 10 mL were then decanted into polypropylene tubes, acidified to pH < 2 with concentrated trace metal grade nitric acid, and held for a minimum of 24 h before analysis. Separate 10 mL aliquots were filtered, immediately after collection, using 0.45 μm membrane filters in a syringe-mounted apparatus.

X-ray Diffraction. We identified crystalline phases in the coupon corrosion scale using X-ray diffraction (XRD). Coupons were dried and analyzed without removing the scale from the surface. We used a Rigaku Ultima IV X-ray diffractometer with a copper Kα radiation source, operated at 35 kV and 30 mA. Scans were acquired over the range 10−70° (2θ) with a step size of 0.04° and a scan speed of 0.8° min^{-1}. The powder diffraction file numbers, corresponding to standards referenced in the article, are listed in Table S3.

X-ray Photoelectron Spectroscopy. The elemental composition of corrosion scale was determined by X-ray photoelectron spectroscopy (XPS) using a Thermo VG Scientific Multilab 2000 instrument. An aluminum X-ray source was used under high vacuum, and a CLAM4 Hemispherical Analyzer with a multichannel detector was used to detect photoelectrons. Survey scans were acquired at a pass energy of 50 eV with a step size of 1.0 eV, and high-resolution scans were acquired at a pass energy of 30 eV with a step size of 0.1 eV. Binding energy was calibrated using the C 1s spectral line, due to adventitious carbon, at 285 eV.

Data Analysis. We used R for data analysis and visualization,[31] along with a collection of widely used contributed packages.[32−35]

Paired Comparisons of Lead Levels at the Point of Use. Paired measurements collected at the point of use in October and February were compared using a parametric test of mean difference for censored data, using the *cen_paired()* function in the *NADA2* package[36] (censoring here refers to lead concentrations below the reporting limit). Duplicate measurements at sites within a single group were averaged; when one was observed and one censored, the duplicate measurements were recensored at the midpoint value. Due to a log transformation of the data, back-transformed group differences are expressed as ratios. R code required to reproduce the analysis is provided in Supporting Information S2, and data are available at doi.org/10.5281/zenodo.5139734.

Equilibrium Lead Solubility Modeling. We modeled equilibrium lead solubility using *tidyphreeqc*,[37] an R interface for PHREEQC,[38] and *pbcusol*,[39] an extension of *tidyphreeqc*. Thermodynamic data relevant to the lead-water-carbonate-orthophosphate system were compiled by Schock et al.[40] (Table S4), and activity coefficients were calculated as described in the PHREEQC manual.[38] Model inputs were pH, orthophosphate, and dissolved inorganic carbon concentration, calculated from pH and alkalinity.[41] We assumed that lead solubility was controlled by hydroxypyromorphite, a mineral that has been identified in lead pipe corrosion scale recovered from the distribution system we studied here.[42]

Because there were not enough paired distribution system data to include aluminum in the model, we fit a separate model to account for aluminum's effect. We calculated hydroxypyromorphite solubility on a grid of orthophosphate and aluminum concentrations at pH 7.5 with 5 mg L^{-1} of dissolved inorganic carbon, assuming that both hydroxypyromorphite and variscite ($AlPO_4 \cdot 2H_2O$) reached an equilibrium with the solution. Thermodynamic data describing variscite dissolution and two aqueous aluminum phosphate species were sourced from a study by Roncal-Herrero and Oelkers,[43] and R code to

https://doi.org/10.1021/acsestwater.1c00320
ACS EST Water 2022, 2, 710−720

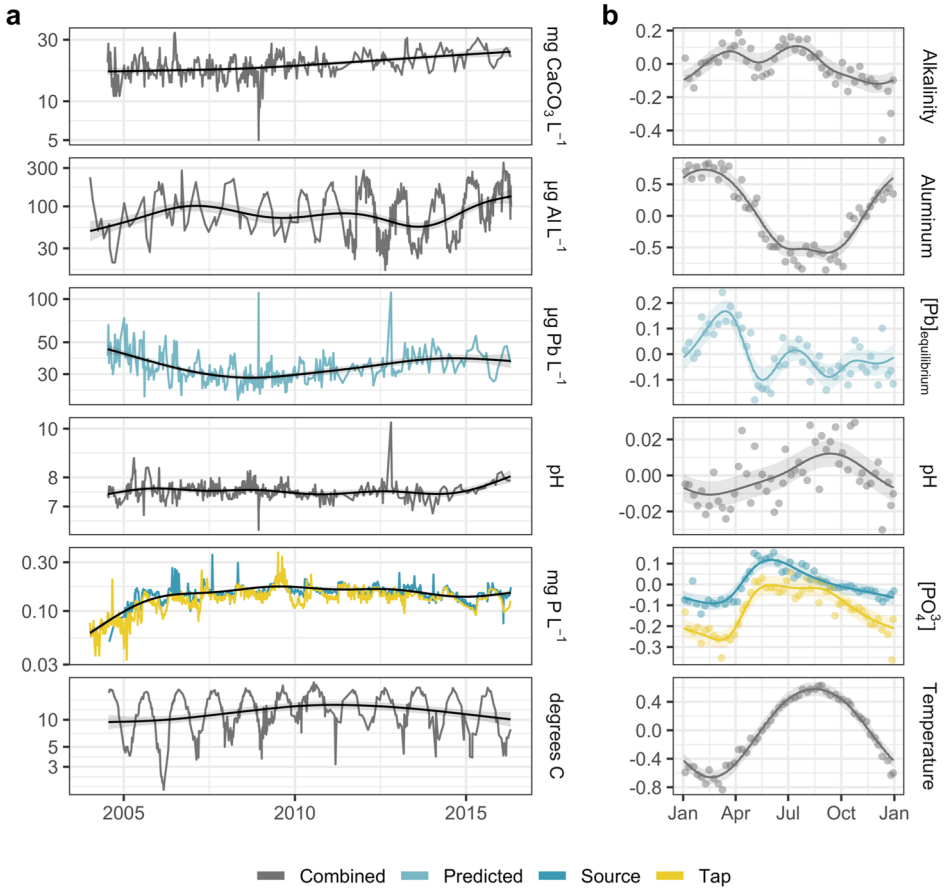

Figure 2. (a) Mean alkalinity (as $CaCO_3$), aluminum, predicted soluble lead, pH, aqueous orthophosphate, and water temperature by date. Due to orthophosphate demand in the distribution system, data are separated by sample location: source (treatment plant) or tap (distribution system). Source and tap are combined in the series representing alkalinity, aluminum, pH, predicted lead, and temperature. The long-term smooth component of the additive fit to the data is superimposed. (b) Seasonal component of each additive model, along with the partial residuals representing the differences between the data and the nonseasonal components of the model, aggregated into weekly means. Both the data and the model are displayed on the transformed scale. Shaded regions represent pointwise 95% confidence intervals on the fitted values.

reproduce the analysis is included in the Supporting Information S3.

Distribution System Monitoring Data. We fit generalized additive models (eqs 1 and 2)[44,45] to a compiled data set comprising fully flushed residential samples, distribution system monitoring samples, and treated water samples collected at the water supply plant. We restricted our analysis to the period when a nominal orthophosphate concentration of 0.5 mg PO_4 L^{-1} was dosed to the system (2003−2016, P dosed as a 3:1 ortho/polyphosphate blend yielding a polyphosphate concentration of approximately 0.04 mg P L^{-1}). Time series included between 10 and 366 measurements per year.

Generalized additive models included a multiyear trend, a seasonal trend, and an autoregressive error term.[46] The multiyear trend was estimated using a thin plate regression spline and the seasonal trend using a cyclic cubic regression spline.[44] We fit separate cyclic splines to orthophosphate data collected at the treatment plant and in the distribution system, and we included a parametric term to model the difference in orthophosphate residual between these two groups. The autoregressive error term was second order in the models fitted to the temperature and orthophosphate product dose series and continuous-time first-order otherwise. Equation 1 describes the basic model.

$$y = \beta_0 + f_{\text{trend}}(t_1) + f_{\text{seasonal}}(t_2) + \epsilon \quad (1)$$

In eq 1, y is the response, t_1 is the numeric date, t_2 is the day of the year, β_0 is the intercept, ϵ is the error term, and the $f(t)$ are linear combinations of basis functions eq 2.

$$f(t) = \sum_{j=1}^{k} b_j(t)\beta_j \quad (2)$$

In eq 2, β_j is the weight associated with the jth basis function. The weighted basis functions $b_j(t)\beta_j$ comprising each model—and their sums, the fitted values—are shown in Figures S2−S4. While the utility data are confidential, we have included the code used to generate the models in the Supporting Information S4, along with a simulated data set. Models are further summarized in Table S5; residuals were approximately Gaussian (Figure S5), homoscedastic (Figures S6−S7), and largely free from autocorrelation (Figure S8).

Static Corrosion Cell Data. We fit a linear regression model to the 2^3 factorial coupon study after a natural log transformation of the response, as described in a foundational text by Montgomery.[47] Model residuals were approximately Gaussian and homoscedastic (Figure S9). A response surface was generated by predicting from the model over a grid of aluminum concentrations, orthophosphate concentrations, and water temperatures. R code to reproduce the results is

https://doi.org/10.1021/acsestwater.1c00320
ACS EST Water 2022, 2, 710−720

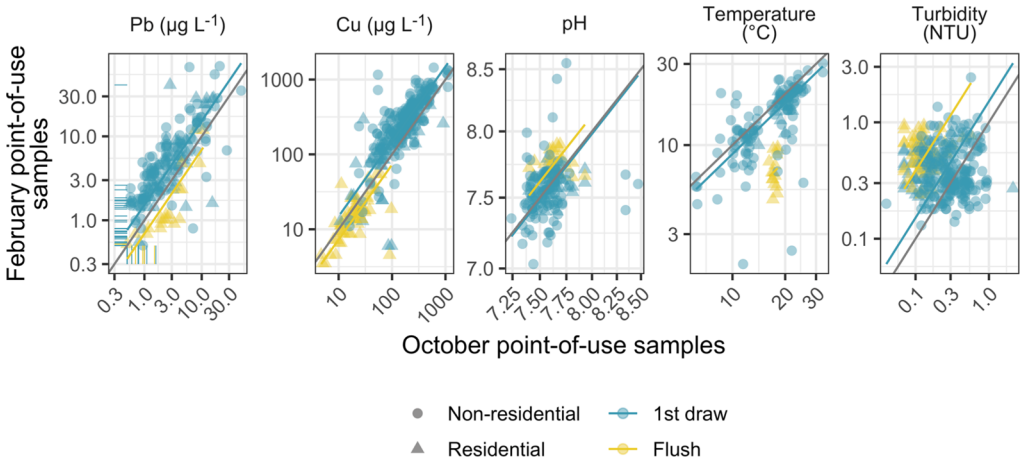

Figure 3. Lead, copper, pH, water temperature, and turbidity at seasonally high (February) and low (October) aluminum concentrations (point-of-use samples). Gray diagonal lines represent $y = x$, and colored diagonal lines represent $y = bx$, where b is the multiplicative pairwise difference estimate (i.e., multiplying the October concentration by b estimates the February concentration). Colored vertical or horizontal lines in the first panel represent left-censored lead measurements.

provided in the Supporting Information S5 and experimental data are available at doi.org/10.5281/zenodo.5139734.

RESULTS AND DISCUSSION

Aluminum and Orthophosphate Seasonality in the Distribution System. Aluminum levels were strongly seasonal in the distribution system we studied (Figure 2). Median aluminum was highest in February and lowest in July: 182 and 32 μg L^{-1}, respectively. The aluminum residual in treated water is generally highest when water temperature is lowest,[21] due largely to the inverse temperature dependence of aluminum hydroxide solubility at the median coagulation pH of 5.75.[6,48,49] Median water temperatures in these two months were 5 and 20 °C.

Orthophosphate also exhibited a seasonal pattern. This is due primarily to variation in the applied corrosion inhibitor dose (Figure S10), but seasonal variation in the reversion rate of polyphosphate may have also been a factor.[50] Minimum and maximum orthophosphate concentrations occurred in February and May, respectively (130 and 170 μg P L^{-1}), approximately opposite to those of aluminum (Figure 2b). Orthophosphate also varied spatially: concentrations were 11% lower in the distribution system compared to the treatment plant, as estimated by a parametric term in the generalized additive model (Table S5). Aluminum precipitates with orthophosphate as $AlPO_4$,[5] which may contribute to this difference and to the seasonal pattern in the distribution system. Alkalinity exhibited a bimodal seasonal pattern, with maxima in March and July and a minimum in December, while seasonal maximum and minimum pH occurred in September and February, respectively.

Seasonal Variation in Predicted Equilibrium Lead Solubility. Variation in orthophosphate, pH, and alkalinity predicted a complex seasonal pattern in equilibrium lead solubility, with two prominent peaks (Figure 2b). The first occurred in March, corresponding to the minimum seasonal orthophosphate concentration and the first of two seasonal alkalinity maxima. The second occurred in July, corresponding to the second seasonal alkalinity maximum. Both peaks in alkalinity yielded corresponding peaks in calculated dissolved inorganic carbon (Figure S10), and at circumneutral pH, equilibrium solubility increases with dissolved inorganic carbon in the presence of orthophosphate.[40] Maximum and minimum predicted lead solubility occurred in March and May, respectively, with mean concentrations of 39 and 27 μg L^{-1}.

Periodic Variation in Lead at the Point of Use. Consistent with equilibrium solubility predictions, lead release exhibited periodic—possibly seasonal—variation concurrent with that of aluminum and opposite to that of orthophosphate. We compared lead levels in the first-drawn samples collected in October with those measured in February at matched sites and drinking water outlets (Figure 3). Lead release into standing water in October was an estimated 65% of that in February ($p \ll 0.001$, $n = 134$, signed-rank test). Copper release exhibited a similar trend: its concentration in standing water in October was an estimated 67% of that in February ($p \ll 0.001$, $n = 134$). These data represent total concentrations, but lead and copper concentrations in 0.45 μm filtrate were an estimated 75 and 89% of the corresponding total concentrations in paired aliquots, respectively, representing 360 samples collected as profiles from residences with full or partial lead service lines (as described in a study by Trueman et al.,[26] Figure S11). This suggests that lead and copper were largely present in the system in forms smaller than 0.45 μm.

On a percentage basis, differences in lead release were larger than expected based on lead solubility—predicted equilibrium lead concentrations were just 8% lower in October compared with February (accounting for variation in pH, alkalinity, and orthophosphate). This discrepancy suggests that factors not captured by the solubility model—processes involving aluminum, for instance—were important. Observed differences were probably not due to water temperature: during overnight stagnation, seasonal temperature variation is significantly damped,[51] and October standing sample temperatures were 113% of February sample temperatures ($p \ll 0.001$, $n = 89$, signed-rank test). If anything, this would tend to increase October lead and copper levels relative to those in February.[52,53]

Colloidal Aluminum and Lead in the Distribution System. While variation in equilibrium lead solubility probably explains at least some of the differences between October and February point-of-use lead levels, particle-generating mechanisms are also likely to be important, including partitioning of lead to particulate (>0.45 μm) or

https://doi.org/10.1021/acsestwater.1c00320
ACS EST Water 2022, 2, 710−720

colloidal (<0.45 μm) aluminum.[20,54,55] Particulate aluminum was seasonal in the distribution system we studied, with the median concentration in October less than half that in February (20 and 48 μg L^{-1}, respectively, Figure 4b). The

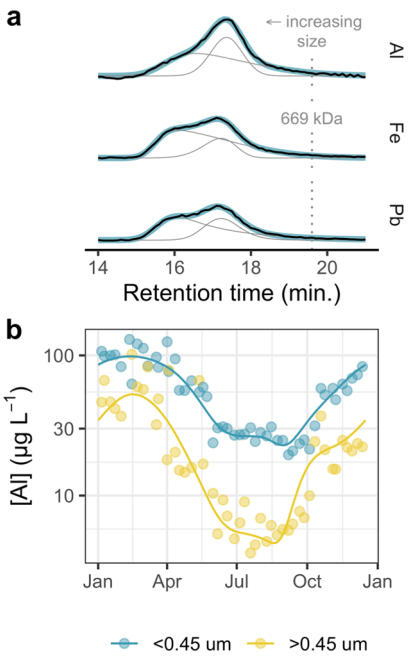

Figure 4. (a) Size exclusion chromatograms representing the relative size distributions of aluminum, iron, and lead. Size distributions were correlated at high apparent molecular weight (n = 16 tap water samples representing 11 homes), and the colloidal fraction shown was sized nominally at 17−450 nm. Intensities have been normalized, baseline-corrected, and summarized as the mean intensity at each retention time. The retention time of thyroglobulin (669 kDa, 17 nm diameter) is indicated by the vertical dashed line. (b) Aluminum in fully flushed residential samples in two size fractions: greater and less than 0.45 μm. Data are aggregated into means by week of the year, and a generalized additive fit to the data with a cyclic cubic regression spline basis is superimposed.

particulate fraction of total aluminum ranged from 16% in August to 35% in February, as estimated from the cyclic cubic regression splines shown in Figure 4b. The variation in particulate aluminum is consistent with turbidity in October being 66 and 26% of that in February in stagnant and flushed point-of-use samples, respectively ($p \ll 0.001$ and $\ll 0.001$, n = 134 and 32, signed-rank tests).

Seasonally varying particulate aluminum concentrations agree with equilibrium aluminum solubility calculations at the expected distribution system's water quality conditions. The aluminum hydroxide phases gibbsite (γ-$Al(OH)_3$), diaspore (α-AlOOH), and boehmite (γ-AlOOH) are all predicted to precipitate at the seasonally high total aluminum concentrations, and variscite ($AlPO_4 \cdot 2H_2O$) is predicted to precipitate seasonally at a dose of 0.5 mg PO_4 L^{-1} (Supporting Information S6).

A fraction of aluminum in 0.45 μm filtrate was colloidal (Figure 4a), which is also consistent with equilibrium solubility predictions. This fraction was sized nominally between 17 nm—the hydrodynamic diameter of thyroglobulin (19.6 min retention time)—and 450 nm—the pore size at which samples were filtered. Colloids in this size range may have served as a mobile sink for lead, promoting release from corrosion scale.

Relative size distributions of lead, aluminum, and iron were typically bimodal (Figure 4a), with two incompletely resolved peaks representing colloids with different apparent molecular weights. Aluminum co-occurred with lead (and iron) in at least one of these two fractions in all samples with detectable aluminum peaks (Figures 4a and S1). This is consistent with previous work documenting adsorption of lead to aluminum hydroxides[56−58] or mixed iron/aluminum (oxyhydr)oxides[59] and with lead and aluminum occurring in a common colloid size fraction.[20,54,55] The presence of aluminum, iron, and lead in distinct but overlapping colloid populations, however, cannot be ruled out completely. Moreover, these data do not provide a complete picture of colloid composition; the role of phosphorus, for example, is not clear.

Potential Impacts of Polyphosphate. Polyphosphates interact strongly with iron, aluminum, manganese, calcium, and lead,[60−65] and the positive effect of polyphosphate complexation on lead solubility is particularly important from a public health perspective. In a different water system, with different water quality, we reported evidence of lead-polyphosphate complexation using the SEC-ICP-MS method summarized above.[42] And while we did not identify similar complexes in samples from more than 20 homes in the system studied here,[20,42] polyphosphate may have influenced lead release in ways that were not apparent from the data. For instance, polyphosphate might have dispersed colloidal iron or aluminum oxides that were also rich in lead,[61,66] which is consistent with the SEC-ICP-MS data that we reported in the previous section (see Colloidal Aluminum and Lead in the Distribution System). Furthermore, because polyphosphates revert to orthophosphate faster at higher temperatures,[67] the polyphosphate concentration in the parts of the system where lead service lines occur may also have been seasonal, with a maximum in winter. Polyphosphate, then, is a possible driver of lead seasonality, although its potential interactions with several other metals preclude a simple model of its effect.

Interaction between Aluminum and Orthophosphate (Lead Coupon Study). Distribution system monitoring data suggest that variation in both aluminum and orthophosphate may have contributed to the seasonal differences in lead release, but it is not clear which factor was more important or to what extent they acted synergistically. We evaluated these factors, along with water temperature, as predictors of lead release using a coupon study. The effect of orthophosphate on equilibrium solubility is relatively well understood, but its interactions with other species to form particles are less well characterized.[68] While polyphosphate may have contributed to seasonal lead release, it was not a focus of the coupon study.

As expected, lead release from coupons increased with water temperature. Raising the cell temperature from 4 to 21 °C caused a 120% increase in geometric mean lead release (Figure 5a), that is, $\overline{[Pb]}_{21\,^\circ C}/\overline{[Pb]}_{4\,^\circ C} - 1 = 1.2$. But while temperature-dependent lead release has been described elsewhere,[26,69] the solubilities of several common lead minerals do not appear to be temperature-sensitive.[52] It is not clear whether changes in solubility, dissolution, complex formation, or particle mobility are primarily responsible for temperature-driven seasonality.[26,40,52,69]

Adding 1 mg PO_4 L^{-1} decreased total lead release by 34% (Figure 5a), while aluminum had the opposite effect: increasing the aluminum concentration from 20 to 500 μg L^{-1} increased total lead release by 41%. Adding orthophosphate and increasing aluminum concentration accompanied a

https://doi.org/10.1021/acsestwater.1c00320
ACS EST Water 2022, 2, 710−720

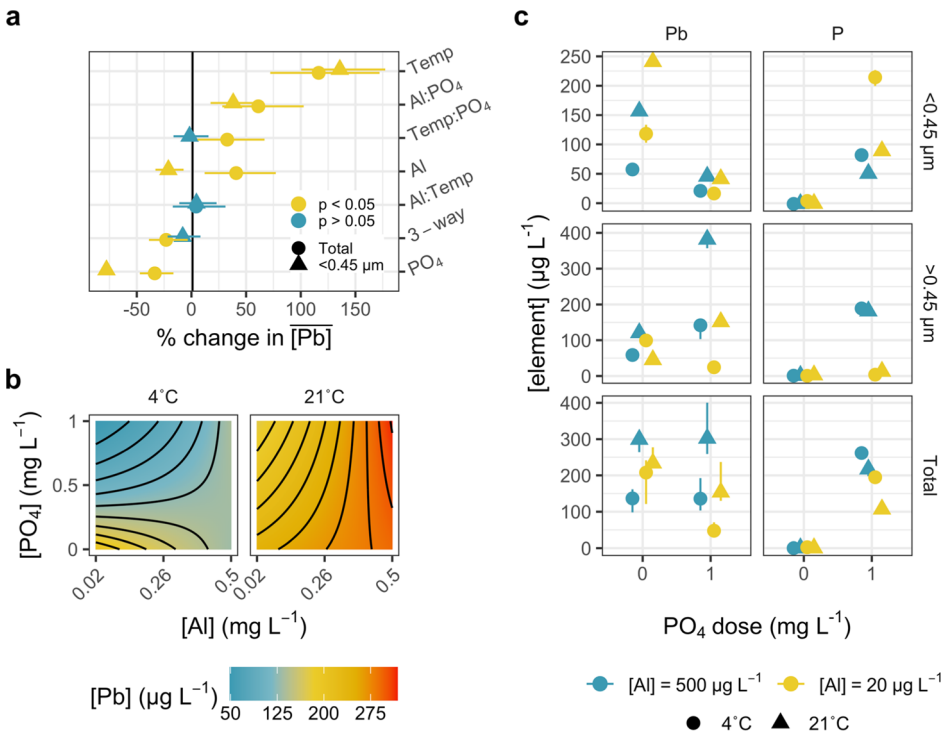

Figure 5. (a) Effect estimates generated by the linear model (lead coupon experiment), along with their 95% confidence intervals. On the *y*-axis, labels with a colon represent two-way interactions estimating the nonadditivity of the main effects; "3-way" represents the three-way interaction effect. (b) Predicted lead concentrations generated by applying the linear regression model to a grid of inputs (aluminum, orthophosphate, and temperature). (c) Median lead and phosphorus in corrosion cells as a function of temperature, aluminum concentration, and orthophosphate dose. Error bars span the interquartile range.

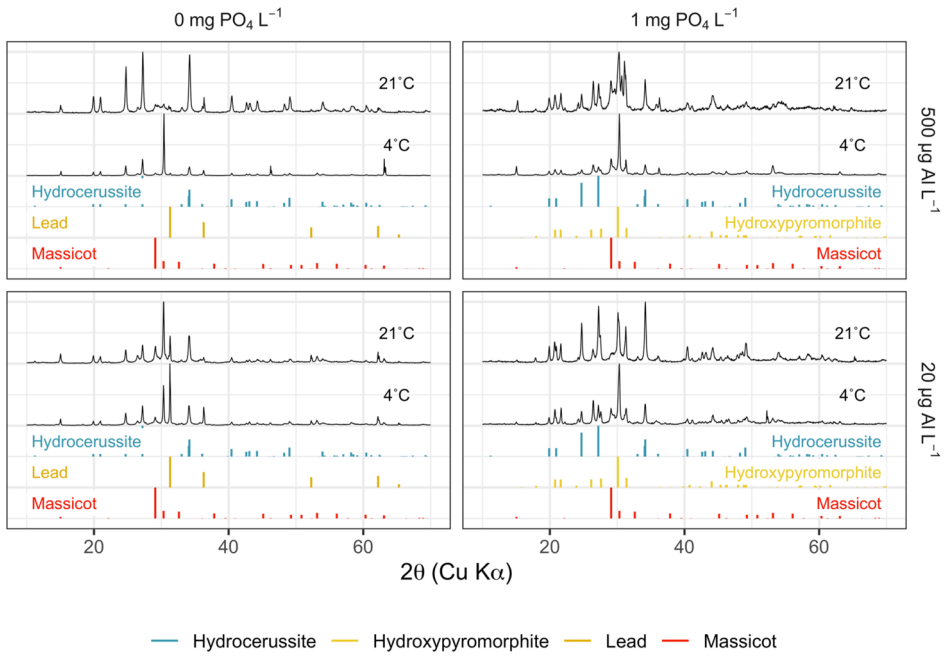

Figure 6. XRD patterns representing corrosion scale on lead coupons at each treatment combination. Intensities are scaled to a [0, 1] interval in all patterns and standards.

further 61% increase in lead. That is, the combined effect of aluminum and orthophosphate was larger than would be expected based on the main effect of each factor. This may be due to the formation of particulate aluminum and phosphorus—perhaps as aluminum phosphate. Particulate phosphorus was highest at the high aluminum level, and in this form, it would presumably be less available to react with lead in a way that immobilized lead at the scale−water interface (Figures 5c and S12). Consistent with this interpretation, substantially less phosphorus was lost to the system at the high aluminum level (i.e., more remained in the water phase). Particulate lead was also greatest at the high

https://doi.org/10.1021/acsestwater.1c00320
ACS EST Water 2022, 2, 710−720

aluminum and orthophosphate levels (Figure 5c), which may be due to partitioning of lead to precipitated aluminum phosphate.

With lead in 0.45 μm filtrate as the response, several effect estimates in the linear model were notably different. Adding orthophosphate, for instance, caused a much larger percentage decrease in filtrate lead levels (78%, Figure 5a). This is consistent with orthophosphate's expected effect on lead solubility, while effective control of particulate lead by orthophosphate requires that lead phosphate precipitates become immobilized in corrosion scale. Here, P/Pb molar ratios were much greater than 1, a threshold that has been noted previously to promote formation of dispersed lead phosphate particles.[68] Moreover, the dispersive effect of orthophosphate may be especially pronounced at the relatively low hardness characteristic of our experimental water (3.9 mg $CaCO_3$ L^{-1}, Table S2). Dispersion is also enhanced in the presence of humic and fulvic acids.[68] And while coagulation here would have removed the majority of the hydrophobic acid fraction,[70] natural organic matter may still have played a role in dispersing particulate lead.[71]

In contrast to its effect on total lead release, aluminum decreased lead in the filtrate by 21% (Figure 5a, neglecting the aluminum−orthophosphate interaction). This agrees with previous work suggesting that aluminum may promote formation of a diffusion barrier on lead composed of aluminum hydroxide, silicate, or other compounds.[11] Alternatively, aluminum may have facilitated partitioning of soluble lead to suspended particles, shifting the size distribution of lead in the test waters.

Coupon Corrosion Scale. We characterized the corrosion scale that formed on coupons under all experimental conditions using XRD (Table S1). As expected, hydroxypyromorphite formed in the presence of orthophosphate, while hydrocerussite ($Pb_3(CO_3)_2(OH)_2$) was identified in scale from all sample coupons. Massicot (β-PbO) was also universally present, but the intensities of the (111) and (200) peaks at 29.1 and 30.3°, respectively, were not consistent with the standard pattern. This may have been due to preferential orientation of crystallites on the coupon surfaces.

Aluminum was not identified in any crystalline mineral forms by XRD, and the experimental patterns representing coupons exposed to 20 and 500 μg Al L^{-1} were similar (Figure 6). Moreover, aluminum was not detectable by XPS in the top few nanometers of corrosion scale exposed to the high level of aluminum (0.5 mg Al L^{-1}) (Figure S13). Thus, it is likely that the aluminum content of scale was relatively low, although XPS detection limits for light elements (e.g., Al) in a heavy element matrix (e.g., Pb) tend to be above 1 atomic percent.[72]

The low surface concentration of aluminum is consistent with our interpretation that aluminum acted primarily by promoting particulate lead formation and limiting the activity of orthophosphate in solution. Moreover, the mineralogy of the scale, as determined by XRD, was predictable without considering the aluminum concentration. On the longer time scales relevant to drinking water distribution, however, aluminum may alter lead corrosion scale in a way that impacts lead release. Here, the apparent effect of aluminum in limiting dissolved lead release in the absence of orthophosphate was relatively small, and it was not due to readily discernible differences in coupon scale at the high and low aluminum levels.

Modeling Aluminum−Phosphate Interactions. Key findings from the coupon study—high lead release from and inhibited phosphorus uptake by corrosion scale in the presence of aluminum—agree well with previous work showing that aluminum interferes with orthophosphate corrosion control.[14] Given our results, this is likely due to both increased solubility and particle-generating mechanisms. And while the full picture is complex, the effect of aluminum on lead solubility—neglecting particles and surfaces—can be modeled by allowing coprecipitation of aluminum and orthophosphate (here as variscite, $AlPO_4{\cdot}2H_2O$) in the presence of hydroxypyromorphite (Figure 7). We applied this model over a grid of

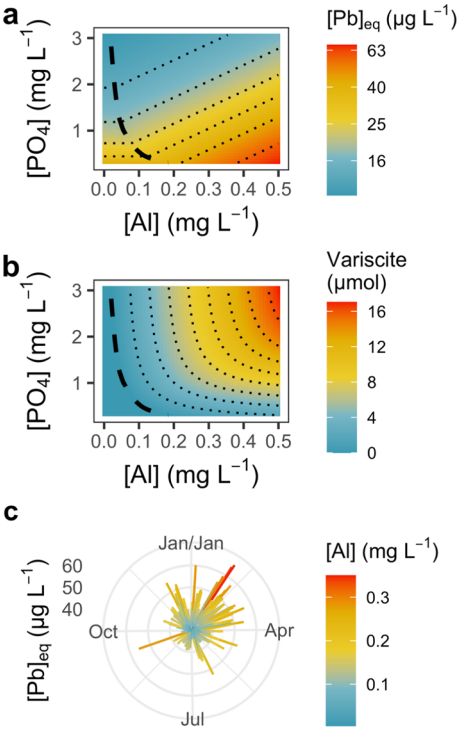

Figure 7. (a) Predicted lead solubility due to dissolution of hydroxypyromorphite, evaluated on a grid of orthophosphate and aluminum concentrations at pH 7.3 with 5 mg L^{-1} of dissolved inorganic carbon. (b) Precipitated variscite, $AlPO_4{\cdot}2H_2O$, at equilibrium under the same conditions. In (a,b), heavy dashed lines represent approximate variscite saturation. (c) Predicted lead solubility by day of the year, using distribution system aluminum data, pH 7.3, 5 mg L^{-1} of dissolved inorganic carbon, and 0.5 mg PO_4 L^{-1} as inputs. N.B., one anomalously high record with 0.96 mg Al L^{-1} is omitted from the plot.

aluminum and orthophosphate concentrations (Figure 7a,b) and, neglecting other sources of variation, to the aluminum concentrations measured in the distribution system (Figure 7c). Consistent with the experimental results, aluminum phosphate precipitation increased lead solubility by decreasing the concentration of orthophosphate in the solution. This was predicted to occur except at very low aluminum concentrations (e.g., approximately 50 μg Al L^{-1} at 1 mg PO_4 L^{-1}, Figure 7b). At the aluminum level characteristic of the distribution system, significant seasonal variation in lead solubility is predicted (Figure 7c).

https://doi.org/10.1021/acsestwater.1c00320
ACS EST Water 2022, 2, 710−720

CONCLUSIONS

We identified an apparent seasonal pattern in lead release into orthophosphate-treated drinking water via point-of-use sampling. And while variation in orthophosphate, pH, and alkalinity predicted a similar pattern in equilibrium lead solubility, seasonal variation in aluminum may have also been a factor, given its correspondence with observed lead levels. In a follow-up coupon corrosion study, aluminum increased total lead release significantly. As expected, orthophosphate decreased lead release, but high levels of aluminum and orthophosphate together resulted in greater lead release than would be predicted based on the main effects of these two factors. We suggest that the interference of orthophosphate corrosion control by aluminum is due largely to precipitation of aluminum phosphate. This reaction limits the activity of orthophosphate and may provide a surface to which soluble lead can partition, thus increasing the total lead content of drinking water.

Our data imply that treatment facilities applying aluminum-based coagulants should ensure that residual aluminum in treated water remains low to limit seasonal variation in the performance of orthophosphate. In the water system we studied, a recent increase in coagulation pH to 6.2 has decreased the median April aluminum concentration at the treatment plant by a factor of more than 4 relative to the 2003−2016 study period. At the more recent concentrations, predicted aluminum phosphate precipitation is minimal (<1 μmol), even at a higher orthophosphate dose of 1 mg PO_4 L^{-1}. The predicted effect of aluminum on equilibrium lead solubility, then, is also much smaller.

More generally, aluminum−orthophosphate−lead interactions highlight an important connection between corrosion control and the treatment process, potentially involving the soluble, colloidal, and particulate fractions of these elements.

ASSOCIATED CONTENT

Supporting Information

The Supporting Information is available free of charge at https://pubs.acs.org/doi/10.1021/acsestwater.1c00320.

Individual SEC chromatograms; details of the generalized additive models fit to water quality time series; additional description of the coupon study; and R code to reproduce the water quality data analysis and the geochemical models (PDF)

AUTHOR INFORMATION

Corresponding Author

Benjamin F. Trueman − *Centre for Water Resources Studies, Department of Civil & Resource Engineering, Dalhousie University, Halifax, Nova Scotia B3H 4R2, Canada;* orcid.org/0000-0002-1539-3092; Phone: 902.494.6070; Email: benjamin.trueman@dal.ca; Fax: 902.494.3105

Authors

Aaron Bleasdale-Pollowy − *Centre for Water Resources Studies, Department of Civil & Resource Engineering, Dalhousie University, Halifax, Nova Scotia B3H 4R2, Canada*

Javier A. Locsin − *Centre for Water Resources Studies, Department of Civil & Resource Engineering, Dalhousie University, Halifax, Nova Scotia B3H 4R2, Canada*

Jessica L. Bennett − *Centre for Water Resources Studies, Department of Civil & Resource Engineering, Dalhousie University, Halifax, Nova Scotia B3H 4R2, Canada*

Wendy H. Krkošek − *Halifax Water, Halifax, Nova Scotia B3K 5M1, Canada*

Graham A. Gagnon − *Centre for Water Resources Studies, Department of Civil & Resource Engineering, Dalhousie University, Halifax, Nova Scotia B3H 4R2, Canada;* orcid.org/0000-0001-5925-2294

Complete contact information is available at: https://pubs.acs.org/10.1021/acsestwater.1c00320

Notes

The authors declare no competing financial interest.

ACKNOWLEDGMENTS

This work was supported by Mitacs through the Mitacs Accelerate Program (Reference # IT23352). We also acknowledge the financial and technical support provided by Halifax Water through the NSERC/Halifax Water Industrial Research Chair program (grant no. IRCPJ: 349838-16) and the technical support provided by Heather Daurie, Andrew George, Caitlin Sampson, and Halifax Water staff.

REFERENCES

(1) Dignam, T.; Kaufmann, R. B.; LeStourgeon, L.; Brown, M. J. Control of Lead Sources in the United States, 1970-2017: Public Health Progress and Current Challenges to Eliminating Lead Exposure. *J. Publ. Health Manag. Pract.* **2019**, *25*, S13−S22.

(2) Zahran, S.; McElmurry, S. P.; Sadler, R. C. Four Phases of the Flint Water Crisis: Evidence from Blood Lead Levels in Children. *Environ. Res.* **2017**, *157*, 160−172.

(3) Colling, J. H.; Whincup, P. A. E.; Hayes, C. R. The Measurement of Plumbosolvency Propensity to Guide the Control of Lead in Tapwaters. *Water Environ. J.* **1987**, *1*, 263−269.

(4) Health Canada. Guidelines for Canadian drinking water quality: Guideline technical document, lead. http://publications.gc.ca/collections/collection_2019/sc-hc/H144-13-11-2018-eng.pdf. (accessed 04 06, 2022).

(5) Frommell, D. M.; Feld, C. M.; Snoeyink, V. L.; Melcher, B.; Feizoulof, C. Aluminum Residual Control Using Orthophosphate. *J.—Am. Water Works Assoc.* **2004**, *96*, 99−109.

(6) Pernitsky, D. J.; Edzwald, J. K. Selection of Alum and Polyaluminum Coagulants: Principles and Applications. *J. Water Supply: Res. Technol.–AQUA* **2006**, *55*, 121−141.

(7) Health Canada. Aluminum in drinking water: Guideline technical document for consultation. https://www.canada.ca/en/health-canada/programs/consultation-aluminum-drinking-water/document.html. (accessed 04 06, 2022).

(8) Mishrra, A.; Wang, Z.; Sidorkiewicz, V.; Giammar, D. E. Effect of Sodium Silicate on Lead Release from Lead Service Lines. *Water Res.* **2021**, *188*, 116485.

(9) Kim, E. J.; Herrera, J. E.; Huggins, D.; Braam, J.; Koshowski, S. Effect of pH on the Concentrations of Lead and Trace Contaminants in Drinking Water: A Combined Batch, Pipe Loop and Sentinel Home Study. *Water Res.* **2011**, *45*, 2763−2774.

(10) Zhang, Y.; Shi, B.; Zhao, Y.; Yan, M.; Lytle, D. A.; Wang, D. Deposition Behavior of Residual Aluminum in Drinking Water Distribution System: Effect of Aluminum Speciation. *J. Environ. Sci.* **2016**, *42*, 142−151.

(11) Snoeyink, V. L.; Schock, M. R.; Sarin, P.; Wang, L.; Chen, A. S.-C.; Harmon, S. M. Aluminium-Containing Scales in Water Distribution Systems: Prevalence and Composition. *J. Water Supply: Res. Technol.–AQUA* **2003**, *52*, 455−474.

(12) Kvech, S.; Edwards, M. Role of Aluminosilicate Deposits in Lead and Copper Corrosion. *J. - Am. Water Works Assoc.* **2001**, *93*, 104−112.
(13) Holmes, H. Probing the Role of Silicates for Corrosion Control in Lead Plumbing. Ph.D Thesis, The University of Western Ontario, 2021.
(14) Li, G.; Bae, Y.; Mishrra, A.; Shi, B.; Giammar, D. E. Effect of Aluminum on Lead Release to Drinking Water from Scales of Corrosion Products. *Environ. Sci. Technol.* **2020**, *54*, 6142−6151.
(15) Crawford, H. B. *Water Quality and Treatement: A Handbook of Community Water Supplies*, 4th ed.; McGraw Hill: Washington, DC, 1990.
(16) Wasserstrom, L. W.; Miller, S. A.; Triantafyllidou, S.; Desantis, M. K.; Schock, M. R. Scale Formation Under Blended Phosphate Treatment for a Utility With Lead Pipes. *J. - Am. Water Works Assoc.* **2017**, *109*, E464−E478.
(17) Doré, E.; Deshommes, E.; Laroche, L.; Nour, S.; Prévost, M. Study of the Long-Term Impacts of Treatments on Lead Release from Full and Partially Replaced Harvested Lead Service Lines. *Water Res.* **2019**, *149*, 566−577.
(18) Doré, E.; Deshommes, E.; Laroche, L.; Nour, S.; Prévost, M. Lead and Copper Release from Full and Partially Replaced Harvested Lead Service Lines: Impact of Stagnation Time Prior to Sampling and Water Quality. *Water Res.* **2019**, *150*, 380−391.
(19) de Mora, S. J.; Harrison, R. M.; Wilson, S. J. The Effect of Water Treatment on the Speciation and Concentration of Lead in Domestic Tap Water Derived from a Soft Upland Source. *Water Res.* **1987**, *21*, 83−94.
(20) Trueman, B. F.; Gagnon, G. A. A New Analytical Approach to Understanding Nanoscale Lead-Iron Interactions in Drinking Water Distribution Systems. *J. Hazard. Mater.* **2016**, *311*, 151−157.
(21) Knowles, A. D.; Nguyen, C. K.; Edwards, M. A.; Stoddart, A.; McIlwain, B.; Gagnon, G. A. Role of Iron and Aluminum Coagulant Metal Residuals and Lead Release from Drinking Water Pipe Materials. *J. Environ. Sci. Health, Part A: Environ. Sci. Eng.* **2015**, *50*, 414−423.
(22) USEPA. *Method 310.2: Alkalinity (Colorimetric, Automated, Methyl Orange) by Autoanalyzer*; NEMI, 1974.
(23) USEPA. *Method 6020b (SW-846): Inductively Coupled Plasma-Mass Spectrometry*, Revision 2; 2014.
(24) American Public Health Association. Standard method 4500-P phosphorus. https://www.standardmethods.org/doi/abs/10.2105/SMWW.2882.093. (accessed 04 06, 2022).
(25) McIlwain, B.. Investigating sources of elevated lead in drinking water. Master's Thesis, Dalhousie University, 2013.
(26) Trueman, B. F.; Camara, E.; Gagnon, G. A. Evaluating the Effects of Full and Partial Lead Service Line Replacement on Lead Levels in Drinking Water. *Environ. Sci. Technol.* **2016**, *50*, 7389−7396.
(27) American Public Health Association. Standard method 3125 Metals by inductively coupled plasma—mass spectrometry. https://www.standardmethods.org/doi/abs/10.2105/SMWW.2882.048. (accessed 04 06, 2022).
(28) Trueman, B. fffprocessr: Process FFF-UV-MALS-ICP-MS data https://github.com/bentrueman/fffprocessr. (accessed 04 06, 2022).
(29) Trueman, B. F.; Anaviapik-Soucie, T.; L'Hérault, V.; Gagnon, G. A. Characterizing Colloidal Metals in Drinking Water by Field Flow Fractionation. *Environ. Sci.: Water Res. Technol.* **2019**, *5*, 2202−2209.
(30) American Public Health Association. Standard method 5310 Total organic carbon (TOC). https://www.standardmethods.org/doi/abs/10.2105/SMWW.2882.104. (accessed 04 06, 2022).
(31) R Core Team. R: A language and environment for statistical computing. https://www.R-project.org/. (accessed 04 06, 2022).
(32) Wickham, H. tidyverse: Easily install and load the 'tidyverse'. https://tidyverse.tidyverse.org/. (accessed 04 06, 2022).
(33) Ram, K.; Wickham, H. Wesanderson: A wes anderson palette generator. https://CRAN.R-project.org/package=wesanderson. (accessed 04 06, 2022).
(34) Grolemund, G.; Wickham, H. Dates and Times Made Easy withlubridate. *J. Stat. Software* **2011**, *40*, 1−25.
(35) Allaire, J.; Xie, Y.; McPherson, J.; Luraschi, J.; Ushey, K.; Atkins, A.; Wickham, H.; Cheng, J.; Chang, W.; Iannone, R. rmarkdown: Dynamic documents for R. https://github.com/rstudio/rmarkdown. (accessed 04 06, 2022).
(36) Julian, P.; Helsel, D. NADA2: Data analysis for censored environmental data. https://CRAN.R-project.org/package=NADA2. (accessed 04 06, 2022).
(37) Dunnington, D. tidyphreeqc: Tidy geochemical modeling using PHREEQC https://github.com/paleolimbot/tidyphreeqc. (accessed 04 06, 2022).
(38) Parkhurst, D. L.; Appelo, C. A. J. Description of Input and Examples for PHREEQC Version 3−a Computer Program for Speciation, Batch-Reaction, One-Dimensional Transport, and Inverse Geochemical Calculations; *Techniques and Methods*; U.S. Geological Survey, 2013; Vol. *6*, p 497.
(39) Trueman, B. pbcusol: Predict lead and copper solubility. https://github.com/bentrueman/pbcusol. (accessed 04 06, 2022).
(40) Schock, M. R.; Wagner, I.; Oliphant, R. J. Corrosion and solubility of lead in drinking water. *Internal Corrosion of Water Distribution Systems*; American Water Works Association Research Foundation: Denver, CO, 1996; pp 131−230.
(41) Schock, M. R. Response of Lead Solubility to Dissolved Carbonate in Drinking Water. *J.—Am. Water Works Assoc.* **1980**, *72*, 695−704.
(42) Trueman, B. F.; Krkošek, W. H.; Gagnon, G. A. Effects of Ortho- and Polyphosphates on Lead Speciation in Drinking Water. *Environ. Sci.: Water Res. Technol.* **2018**, *4*, 505−512.
(43) Roncal-Herrero, T.; Oelkers, E. H. Does Variscite Control Phosphate Availability in Acidic Natural Waters? An Experimental Study of Variscite Dissolution Rates. *Geochim. Cosmochim. Acta* **2011**, *75*, 416−426.
(44) Wood, S. N. *Generalized Additive Models: An Introduction with R*, 2nd ed.; Chapman; Hall/CRC, 2017.
(45) Simpson, G. L. gratia: Graceful 'ggplot'-based graphics and other functions for GAMs fitted using 'mgcv'. https://gavinsimpson.github.io/gratia/. (accessed 04 06, 2022).
(46) Pinheiro, J.; Bates, D.; DebRoy, S.; Sarkar, D.; R Core Team. nlme: Linear and nonlinear mixed effects models. https://CRAN.R-project.org/package=nlme. (accessed 04 06, 2022).
(47) Montgomery, D. C. *Design and Analysis of Experiments*, 8th ed.; John Wiley & Sons, Inc: Hoboken, NJ, 2013.
(48) Knowles, A. D.; MacKay, J.; Gagnon, G. A. Pairing a Pilot Plant to a Direct Filtration Water Treatment Plant. *Can. J. Civ. Eng.* **2012**, *39*, 689−700.
(49) Vadasarukkai, Y. S. Investigation of the mixing energy consumption affecting coagulation and floc aggregation. PhD Thesis, Dalhousie University, Halifax, Nova Scotia, 2016.
(50) Cantor, A. F.; Denig-Chakroff, D.; Vela, R. R.; Oleinik, M. G.; Lynch, D. L. Use of Polyphosphate in Corrosion Control. *J.—Am. Water Works Assoc.* **2000**, *92*, 95−102.
(51) Britton, A.; Richards, W. Factors influencing plumbsolvency in Scotland. *J. Inst. Water Eng. Sci.* **1981**, *35*, 349−364.
(52) Masters, S.; Welter, G. J.; Edwards, M. Seasonal Variations in Lead Release to Potable Water. *Environ. Sci. Technol.* **2016**, *50*, 5269−5277.
(53) Boulay, N.; Edwards, M. Role of Temperature, Chlorine, and Organic Matter in Copper Corrosion by-Product Release in Soft Water. *Water Res.* **2001**, *35*, 683−690.
(54) Aghasadeghi, K.; Peldszus, S.; Trueman, B. F.; Mishrra, A.; Cooke, M. G.; Slawson, R. M.; Giammar, D. E.; Gagnon, G. A.; Huck, P. M. Pilot-Scale Comparison of Sodium Silicates, Orthophosphate and pH Adjustment to Reduce Lead Release from Lead Service Lines. *Water Res.* **2021**, *195*, 116955.
(55) Li, B.; Trueman, B. F.; Munoz, S.; Locsin, J. M.; Gagnon, G. A. Impact of Sodium Silicate on Lead Release and Colloid Size Distributions in Drinking Water. *Water Res.* **2021**, *190*, 116709.

https://doi.org/10.1021/acsestwater.1c00320
ACS EST Water 2022, 2, 710−720

(56) Kinniburgh, D. G.; Jackson, M. L.; Syers, J. K. Adsorption of Alkaline Earth, Transition, and Heavy Metal Cations by Hydrous Oxide Gels of Iron and Aluminum. *Soil Sci. Soc. Am. J.* **1976**, *40*, 796−799.
(57) McBride, M. B. Processes of Heavy and Transition Metal Sorption by Soil Minerals. *Interactions at the Soil Colloid—Soil Solution Interface*; Springer, 1991; pp 149−175.
(58) Saha, U. K.; Taniguchi, S.; Sakurai, K. Adsorption Behavior of Cadmium, Zinc, and Lead on Hydroxyaluminum- and Hydroxyaluminosilicate-Montmorillonite Complexes. *Soil Sci. Soc. Am. J.* **2001**, *65*, 694−703.
(59) Violante, A.; Ricciardella, M.; Pigna, M. Adsorption of Heavy Metals on Mixed Fe-Al Oxides in the Absence or Presence of Organic Ligands. *Water, Air, Soil Pollut.* **2003**, *145*, 289−306.
(60) De Kort, E.; Minor, M.; Snoeren, T.; Van Hooijdonk, T.; Van Der Linden, E. Calcium-Binding Capacity of Organic and Inorganic Ortho- and Polyphosphates. *Dairy Sci. Technol.* **2009**, *89*, 283−299.
(61) Wan, B.; Elzinga, E. J.; Huang, R.; Tang, Y. Molecular Mechanism of Linear Polyphosphate Adsorption on Iron and Aluminum Oxides. *J. Phys. Chem. C* **2020**, *124*, 28448−28457.
(62) Wan, B.; Huang, R.; Diaz, J. M.; Tang, Y. Manganese Oxide Catalyzed Hydrolysis of Polyphosphates. *ACS Earth Space Chem.* **2019**, *3*, 2623−2634.
(63) Holm, T. R.; Smothers, S. H. Characterizing the Lead-Complexing Properties of Polyphosphate Water Treatment Products by Competing-Ligand Spectrophotometry Using 4-(2-Pyridylazo)-Resorcinol. *Int. J. Environ. Anal. Chem.* **1990**, *41*, 71−82.
(64) Edwards, M.; McNeill, L. S. Effect of Phosphate Inhibitors on Lead Release from Pipes. *J.—Am. Water Works Assoc.* **2002**, *94*, 79−90.
(65) Li, B.; Trueman, B. F.; Locsin, J. M.; Gao, Y.; Rahman, M. S.; Park, Y.; Gagnon, G. A. Impact of Sodium Silicate on Lead Release from Lead(II) Carbonate. *Environ. Sci.: Water Res. Technol.* **2021**, *7*, 599−609.
(66) Bollyn, J.; Nijsen, M.; Baken, S.; Joye, I.; Waegeneers, N.; Cornelis, G.; Smolders, E. Polyphosphates and Fulvates Enhance Environmental Stability of PO_4-Bearing Colloidal Iron Oxyhydroxides. *J. Agric. Food Chem.* **2016**, *64*, 8465−8473.
(67) Strauss, U. P.; Treitler, T. L. Degradation of Polyphosphates in Solution. I. Kinetics and Mechanism of the Hydrolysis at Branching Points in Polyphosphate Chains. *J. Am. Chem. Soc.* **1956**, *78*, 3553−3557.
(68) Zhao, J.; Giammar, D. E.; Pasteris, J. D.; Dai, C.; Bae, Y.; Hu, Y. Formation and Aggregation of Lead Phosphate Particles: Implications for Lead Immobilization in Water Supply Systems. *Environ. Sci. Technol.* **2018**, *52*, 12612−12623.
(69) Cartier, C.; Laroche, L.; Deshommes, E.; Nour, S.; Richard, G.; Edwards, M.; Prévost, M. Investigating Dissolved Lead at the Tap Using Various Sampling Protocols. *J.—Am. Water Works Assoc.* **2011**, *103*, 55−67.
(70) Korshin, G. V.; Ferguson, J. F.; Lancaster, A. N.; Wu, H. *Corrosion and Metal Release for Lead-Containing Materials: Influence of NOM; AWWA Research Foundation*; American Water Works Association: Denver, 1999.
(71) Liu, H.; Schonberger, K. D.; Korshin, G. V.; Ferguson, J. F.; Meyerhofer, P.; Desormeaux, E.; Luckenbach, H. Effects of Blending of Desalinated Water with Treated Surface Drinking Water on Copper and Lead Release. *Water Res.* **2010**, *44*, 4057−4066.
(72) Shard, A. G. Detection Limits in XPS for More Than 6000 Binary Systems Using Al and Mg Kα X-Rays: XPS Detection Limits. *Surf. Interface Anal.* **2014**, *46*, 175−185.

https://doi.org/10.1021/acsestwater.1c00320
ACS EST Water 2022, 2, 710−720